AD-A045 628 EG AND G INC SALEM MASS F/G 9/5
REPETITIVE SERIES INTERRUPTER II.(U)
JUL 77 R SIMON, D V TURNQUIST DAAB07-76-C-1301
UNCLASSIFIED ECOM-76-1301-4 NL

1 OF 1
AD A045628

END
DATE FILMED
11-77
DDC

(12)

Research and Development Technical Report

ECOM -76-1301-4

REPETITIVE SERIES INTERRUPTER II

Robert Simon
David V. Turnquist
EG&G Inc.
Electronic Components Division
Salem, Massachusetts 01970

July 1977

Fourth Triannual Report for the Period 1 March 1977 to 31 May 1977

Prepared for:

ECOM

US ARMY ELECTRONICS COMMAND FORT MONMOUTH, NEW JERSEY 07703

NOTICES

Disclaimers

The findings in this report are not to be construed as an official Department of the Army position, unless so designated by other authorized documents.

The citation of trade names and names of manufacturers in this report is not to be construed as official Government indorsement or approval of commercial products or services referenced herein.

Disposition

Destroy this report when it is no longer needed. Do not return it to the originator.

UNCLASSIFIED
SECURITY CLASSIFICATION OF THIS PAGE (When Data Entered)

REPORT DOCUMENTATION PAGE

READ INSTRUCTIONS BEFORE COMPLETING FORM

1. REPORT NUMBER: ECOM-76-1301-4	2. GOVT ACCESSION NO.
3. RECIPIENT'S CATALOG NUMBER	
4. TITLE (and Subtitle): Repetitive Series Interrupter II,	5. TYPE OF REPORT & PERIOD COVERED: [redacted] Triannual Report, NO. 4, 1 Mar [redacted] 31 May 77
6. PERFORMING ORG. REPORT NUMBER	
7. AUTHOR(s): Robert Simon, David V. Turnquist	8. CONTRACT OR GRANT NUMBER(s): DAAB07-76-C-1301
9. PERFORMING ORGANIZATION NAME AND ADDRESS: EG&G Inc., 35 Congress Street, Salem, Massachusetts 01970	10. PROGRAM ELEMENT, PROJECT, TASK AREA & WORK UNIT NUMBERS: 62705 E1, 1L762705AH94 E1.01
11. CONTROLLING OFFICE NAME AND ADDRESS: US Army Electronics Command, ATTN: DRSEL-TL-BG, Fort Monmouth, New Jersey 07703	12. July 77
	13. NUMBER OF PAGES: 54 47p.
14. MONITORING AGENCY NAME & ADDRESS (if different from Controlling Office)	15. SECURITY CLASS. (of this report): Unclassified
	15a. DECLASSIFICATION/DOWNGRADING SCHEDULE

16. DISTRIBUTION STATEMENT (of this Report)

Approved for Public Release; Distribution Unlimited

17. DISTRIBUTION STATEMENT (of the abstract entered in Block 20, if different from Report)

18. SUPPLEMENTARY NOTES

19. KEY WORDS (Continue on reverse side if necessary and identify by block number)

Series Interrupter
Gas Filled Device
Fuse
Thyratron
Magnetic Interaction Region

20. ABSTRACT (Continue on reverse side if necessary and identify by block number)

Further development of the Repetitive Series Interrupter, a hydrogen thyratron modified for opening-switch operation, is described. Deuterium is rejected as an alternative fill gas because of increased interrupting magnetic field requirements due to the greater inertial resistance of the heavier positive ions to the magnetic field-induced transverse diffusion. Modified magnetic field pulse shapes are explored, and an analysis of a positive column of weakly ionized hydrogen gas in a transverse magnetic field is presented.

DD FORM 1 JAN 73 1473 EDITION OF 1 NOV 65 IS OBSOLETE

UNCLASSIFIED
SECURITY CLASSIFICATION OF THIS PAGE (When Data Entered)

ABBREVIATIONS AND SYMBOLS

Bq	Magnetic field (kilogauss) required for reducing fault current to zero
Ebb	Main supply voltage for tube under test
Ef	TUT cathode heater filament voltage
ξj	Magnetic field energy for RSI tube volume
Em	Magnet supply voltage
epy	Instantaneous full voltage across tube under test
Eres	TUT hydrogen reservoir voltage
Eq	Magnet circuit voltage required for quenching fault current
etd	TUT voltage drop during normal pulse operation
ib	Peak RSI-carried current
iRSI	RSI-carried current, as a function of time
L	Length of interaction tube used during test
m	Empirical exponent of proportionality between Bq and 1/L
MCCD	Magnetic-Controlled Charging Diode
N	Number of turns in magnet coil
P	TUT pressure
prr	TUT pulse repetition rate
r	Radius of interaction tube
Rcct	Resistance of magnetic field probe circuit
Rchoke	Resistance of magnetic field probe circuit intergrating inductor
Rm	Magnet circuit load resistance
Rl	Pulse-forming network load resistance
Rrc	Fault network load resistance
τD	Time delay between TUT fire and magnet fire
τr	Magnetic field risetime
TUT	Tube under test
β	Empirical exponent of proportionality between Bq and Ebb
δ	Empirical exponent of proportionality between Bq and ib
Δtad	Full range of deviation of delay time drift for tube fire

SYMBOLS USED IN POSITIVE COLUMN ANALYSIS

a	Discharge diameter during magnetic constriction
b	Discharge breadth during magnetic constriction
B	Magnetic field strength
D	Electron diffusion coefficient
$\vec{E}$	Electric field
$E_{x,y,z}$	Electric field components
f	Average fraction of energy lost by an electron in a neutral particle collision
f_i	Ionization rate per electron
$\vec{J}$	Current density
$J_{x,y,z}$	Current density components
k	Boltzmann's constant
$L_{x,y,z}$	Positive column dimensions
m_e	Electron mass
$n_{e,i}$	Electron, ion concentration
$T_{e,i}$	Electron, ion temperature
x_*	Position of maximum electron density
$\vec{V}_{e,i}$	Electron, ion velocities
Z	Atomic number of gas species (for hydrogen set = 1)
α, β	Parameters derived in the solution of the equation for n_e
Λ	Characteristic diffusion length
$\mu_{e,i}$	Electron, ion mobility $= \dfrac{e}{m_{e,i}\,\nu_{ce,ci}}$
$\nu_{ce,ci}$	Collision frequency of electrons, ions with neutral hydrogen
ν_i	Electron ionization frequency

TABLE OF CONTENTS

LIST OF ILLUSTRATIONS

1. INTRODUCTION

1.1 FOREWORD

This report constitutes the Fourth Triannual Report under USAECOM Contract DAAB07-C-1301, entitled "Repetitive Series Interrupter II." The investigations herein described were performed from 1 March 1977 through 30 April 1977 by EG&G, Inc., 35 Congress Street, Salem, Massachusetts.

1.2 BACKGROUND

It has been shown that Repetitive Series Interrupter (RSI) tubes are capable of interrupting high voltage D.C. discharges by the superposition of a high transverse magnetic field across the interaction channel in the body of the tube. Experimentation with uniform diameter discharge columns has shown that the magnetic field required for such interruption in hydrogen varies approximately according to the equation $Bq = L^{-0.75} Ebb^{1.25} ib^{0.25}$ (Bq in kilogauss, L in cm, Ebb in kV, ib in amperes). A 67% reduction in Bq was observed for a tube with a nonuniform diameter discharge channel (RSI 005) composed of a series of "plasma chute" wall spacings for increasing the plasma-wall interaction.

Present problems confronting the RSI development effort include: (1) the simultaneous assurance of low voltage drop in the RSI tube during pulsed operation and of minimal level of magnetic field energy required for the interruption of a fault discharge; (2) the prevention of restriking of the fault discharge after interruption; and (3) the assurance of stable, jitter-free, moderately high pulse rate normal operation.

1.3 PRESENT RESULTS

Present work was principally directed toward problems (1) and (2) listed above. Principal tubes under study were RSI 004 (Figure 1) and RSI 005 (Figure 2). A test with deuterium as the fill gas was made to determine whether the probable advantage of lower voltage drop in deuterium would not be counterbalanced by an increase in the required quenching magnetic field. Results were not encouraging, since the interrupting magnetic field energy required for a deuterium tube is 2 to 4 times higher than that for a hydrogen-filled tube, due to the greater inertial resistance of the increased mass to the magnetic-field-induced transverse diffusion.

Use of a "plasma chute" type design had previously suggested a significant reduction in the required magnetic quenching field, but testing has been limited to low voltages by extraneous internal arcing. The attempt to eliminate the arcing by reducing the glass to ceramic gap fractured the glass envelope of the tube. An examination was made of the damage sustained by the internal ceramic components. Localized fusion and erosion of the ceramic disks was noted on the corners and the surface facing the cathode. Since the voltage drop is rising rapidly during interruption, the cause may be increased electron energy.

Magnetic pulse-shaping with a high initial peak followed by a several hundred microsecond low field was used in an effort to eliminate restriking after interruption of the fault discharge. Efforts to date in deuterium seem to indicate that pulse-shaping has a greater effect on delaying the restrike by several hundred microseconds than on eliminating it. More attention must be paid to the external circuitry with respect to the trigger circuit, grid bias, and transient voltage elimination, in conjunction with magnetic pulse-shaping to eliminate restriking.

A preliminary theoretical analysis of the positive column in a transverse magnetic field has been completed and is included in this report. Detailed comparisons of the results of the analysis with experimental results have not

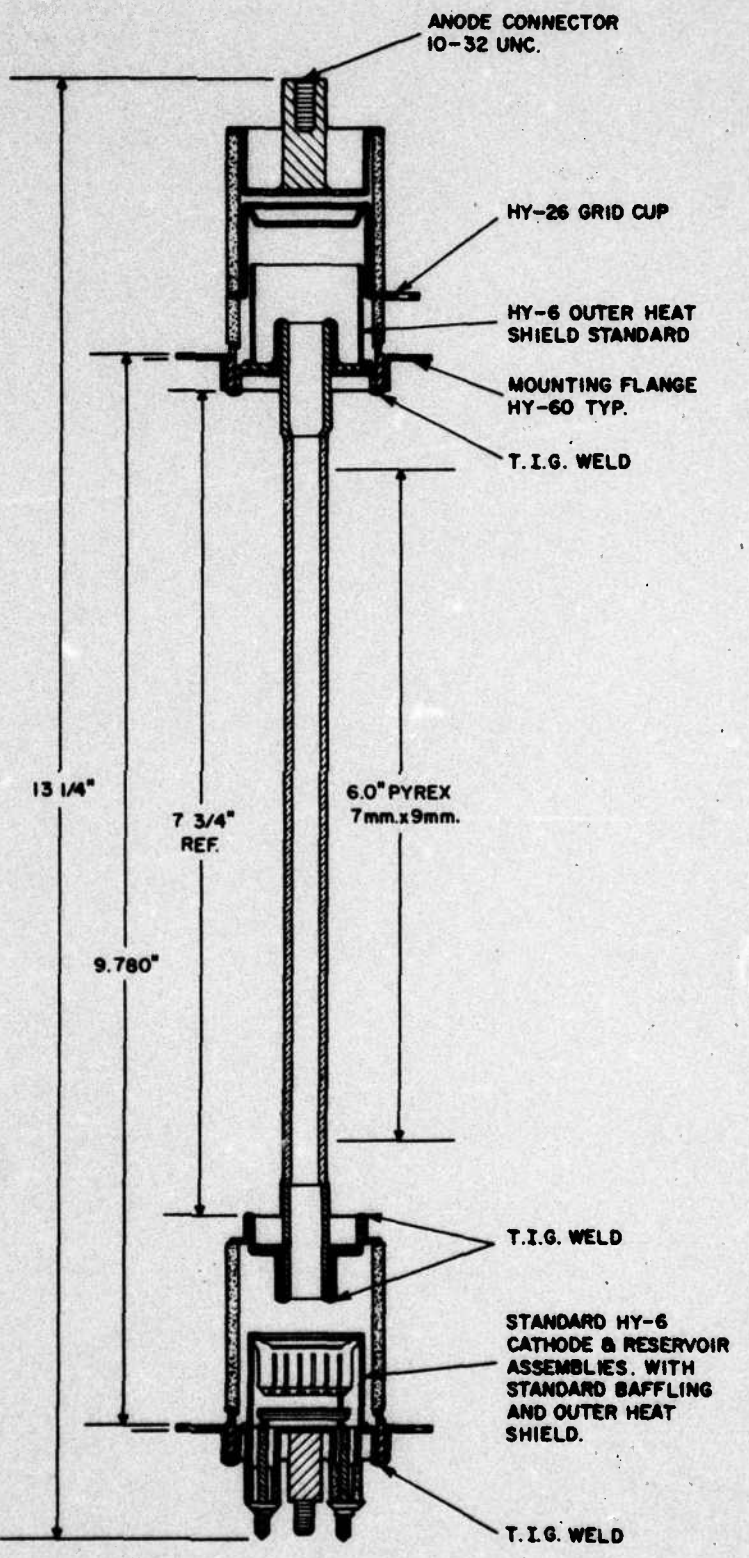

NOTES:

1. LOWER PAN ASS'Y IS STD. EXCEPT FOR THE GRID FEEDTHRU REPLACED WITH STEEL STUD.
2. RESISTANCE READINGS REF. # 84216.

Figure 1. Tube RSI 004.

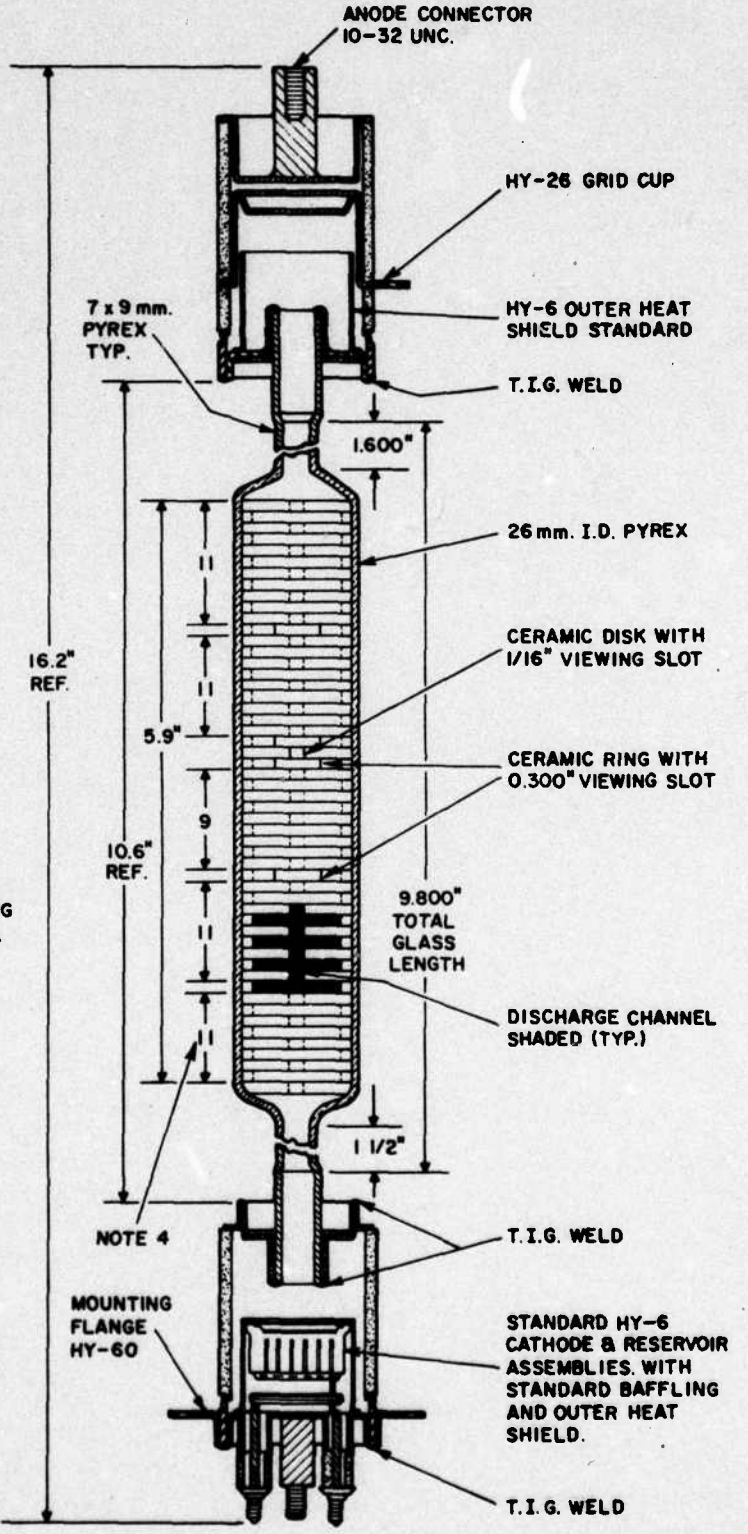

NOTES:

1. LOWER PAN ASS'Y IS STD. EXCEPT FOR THE GRID FEEDTHRU REPLACED WITH STEEL STUD.
2. CERAMIC STACK CONSISTS OF 59 CERAMICS-ALTERNATING FROM 0.130 I.D. TO 0.800" I.D.
3. NOTE (6) VIEWING SLOTS, (5) ≈0.300" WIDE AND (1) ≃ 1/16" WIDE, SLOTS ARE NOT PERFECTLY ALIGNED AS SHOWN.
4. NUMBERS INDICATE QTY. OF CERAMICS BETWEEN VIEWING SLOTS.

Figure 2. Tube RSI 005.

yet been made, but the overall conclusion that a discharge column constricts in a transverse field agrees with observations.

For a practical RSI tube, power dissipation in the protected device during fault interruption is of critical importance. Presuming an arc voltage of 100 volts in the protected device, a total charge transfer, Q, of less than 0.01 coulomb would result in an energy dissipation of 0.15 joule in that device. Previous results indicate that a 300-ampere discharge is interruptible in less than 10 microseconds, with a charge transfer $Q = \frac{1}{2} It = 0.0015$ coulomb. This result is well within safety requirements.

2. PROGRESS

2.1 DEUTERIUM TESTING

In 1969, L. N. Breusova[1] reported a study comparing the voltage drops of hydrogen and deuterium in the positive column of a gas discharge. He found that the voltage drop was a strong function of the choice of gas, the tube pressure, and the discharge current, as well as the choice of operation in pulsed or D.C. mode (Figures 3a-3d). This work was done with a 30-microsecond pulse length in an 18.5-mm diameter discharge tube. A comparison of his results with ours can be made by plotting E/p versus rp, as in Figure 3a.

It is apparent that our results agree well with his. The RSI 003 voltage drop values can be considered more reliable than those of RSI 001, since they result from measurements in a discharge channel of varying length. The disparity previously reported (Second Triannual Report) between the RSI data and that of Brown[2] is therefore resolved as a matter of different current densities in the plasma discharge.

It is immediately suggestive that deuterium or a still heavier gas might prove valuable for use in the RSI tubes, since the tube drop appears to diminish somewhat as the reciprocal of the square root of the ion mass. However, problems arise with current quenching in the heavier gases, since the heavier positive ions have a greater inertial resistance to the magnetic field-induced transverse diffusion, thereby slowing plasma movement to the plasma-interaction wall surface. To determine the effects of deuterium on current interruption, RSI 004 (Figure 1) was refilled with deuterium and tested, with

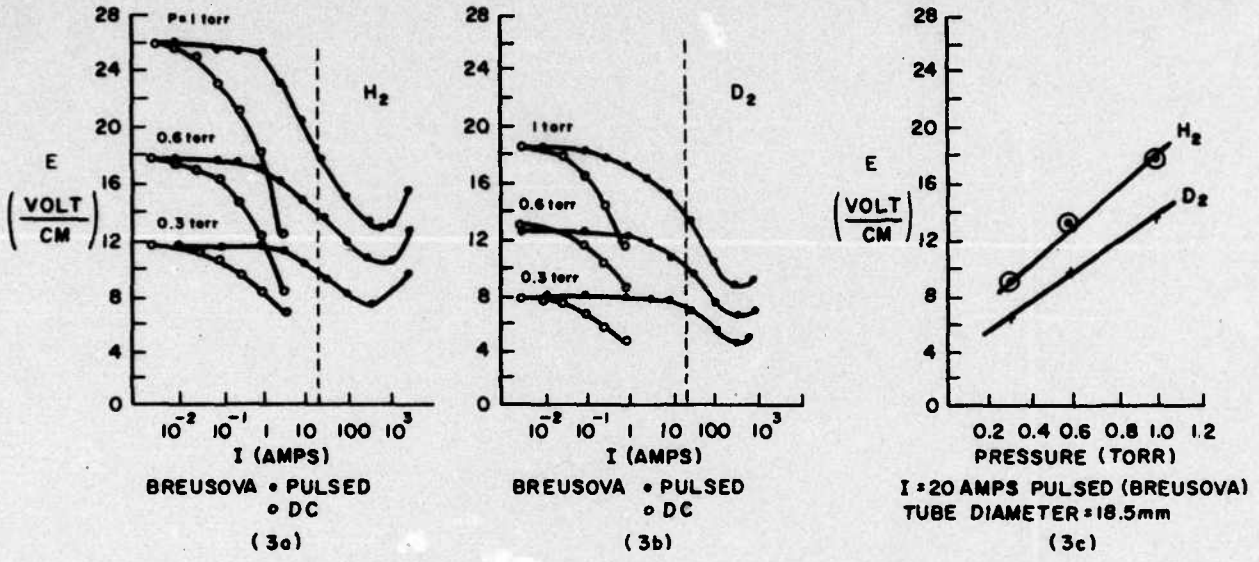

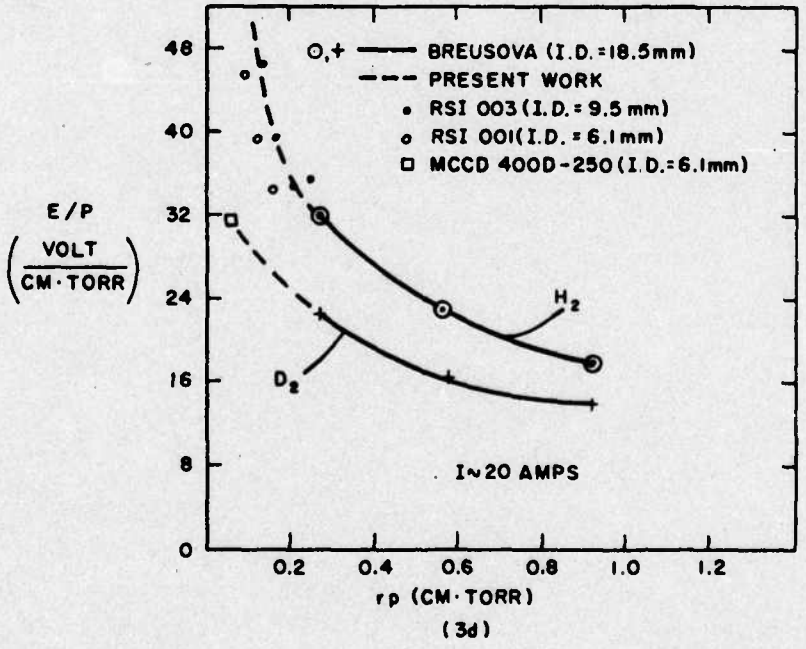

Figure 3. Voltage drop vs. current and pressure: comparison of results.

the required interrupting magnetic fields as shown in Figure 4. Several values of the ratio of interrupting magnetic field of deuterium to that of hydrogen ($Bq(D_2)/Bq(H_2)$) for various voltage and current levels are given in Figure 5. The average of these values is 1.67, but higher ratios appear at higher current and voltage levels.

The voltage drop advantage of deuterium over hydrogen in the positive column was determined by Breusova to be a reduction of approximately 1/1.4. Results from our tests yielded a ratio of about 1/1.5. To achieve the same tube drop, then, a hydrogen tube could be lengthened by a factor of about 1.5 when filled with deuterium. Using previously obtained results, that the quenching field varies approximately as $L^{-0.75}$ (L = interaction length), the ratio of quenching fields of deuterium to hydrogen tubes would equal approximately $1.67/(1.5^{-0.75}) = 1.35$. The magnetic field energy, proportional to Bq^2L, would give a ratio for the two tubes = $(1.35)^2\ 1.5$ = about 2.3. Therefore, the use of deuterium in the RSI application offers no advantage, even with the consideration of reduced tube drop. Deuterium-filling would be advised only in applications where the tube voltage drop was of paramount importance.

Hydrogen, therefore, is the gas of choice for present RSI tubes. Furthermore, it appears that any heavier gas (or metal vapor) would only make current interruption more difficult. Low concentration impurities in the discharge may, for the same reason, impair current interrupting capability.

2.2 RSI 005 ANALYSIS

Tube RSI 005, shown in cross-section in Figure 2, has an interaction region composed of a glass tube envelope within which are stacked a series of ceramic washers of alternating large and small internal diameter base, in an attempt to modulate the interaction wall surface. As reported earlier,

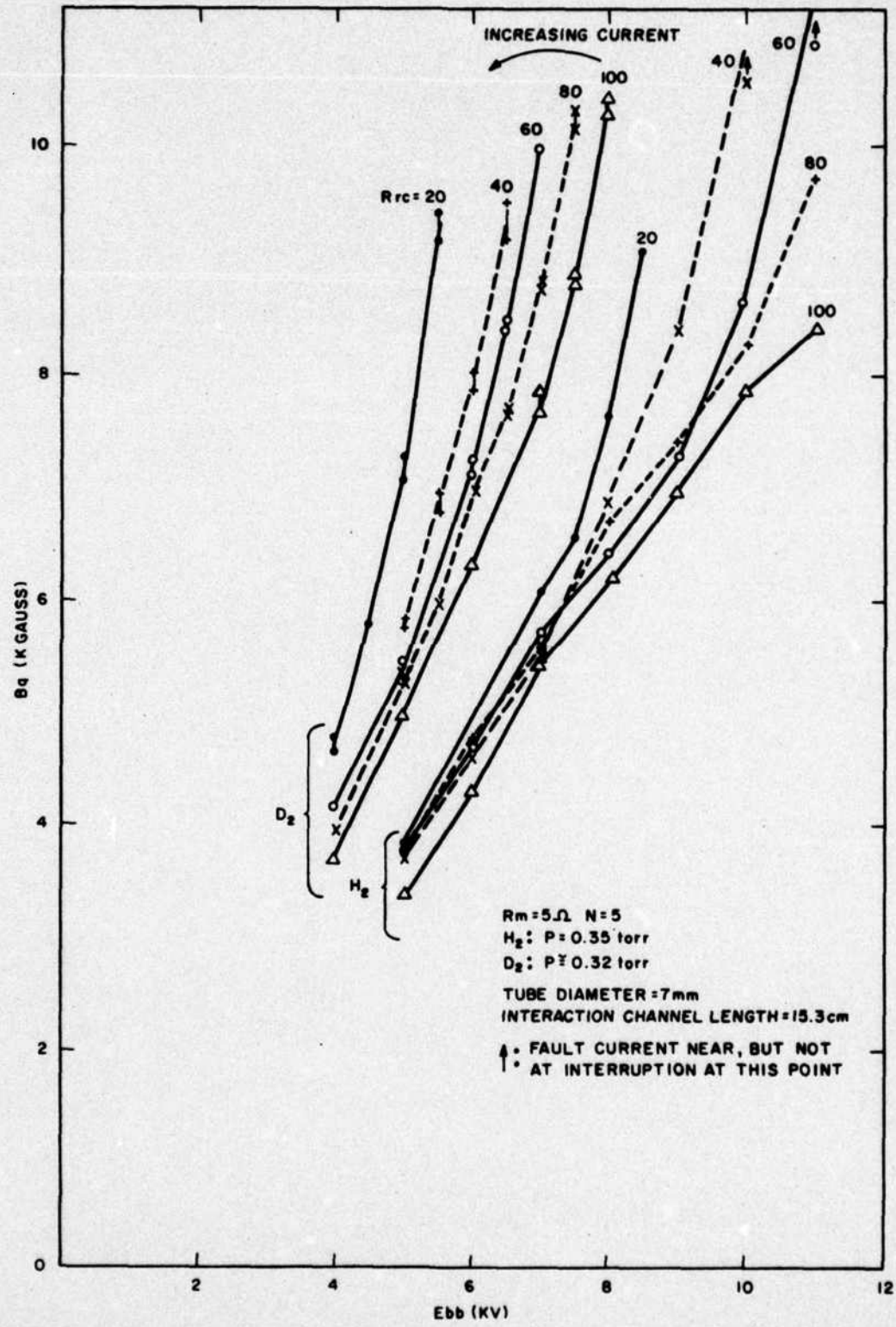

Figure 4. Bq vs. Ebb, Rrc for RSI 004: D_2 vs. H_2.

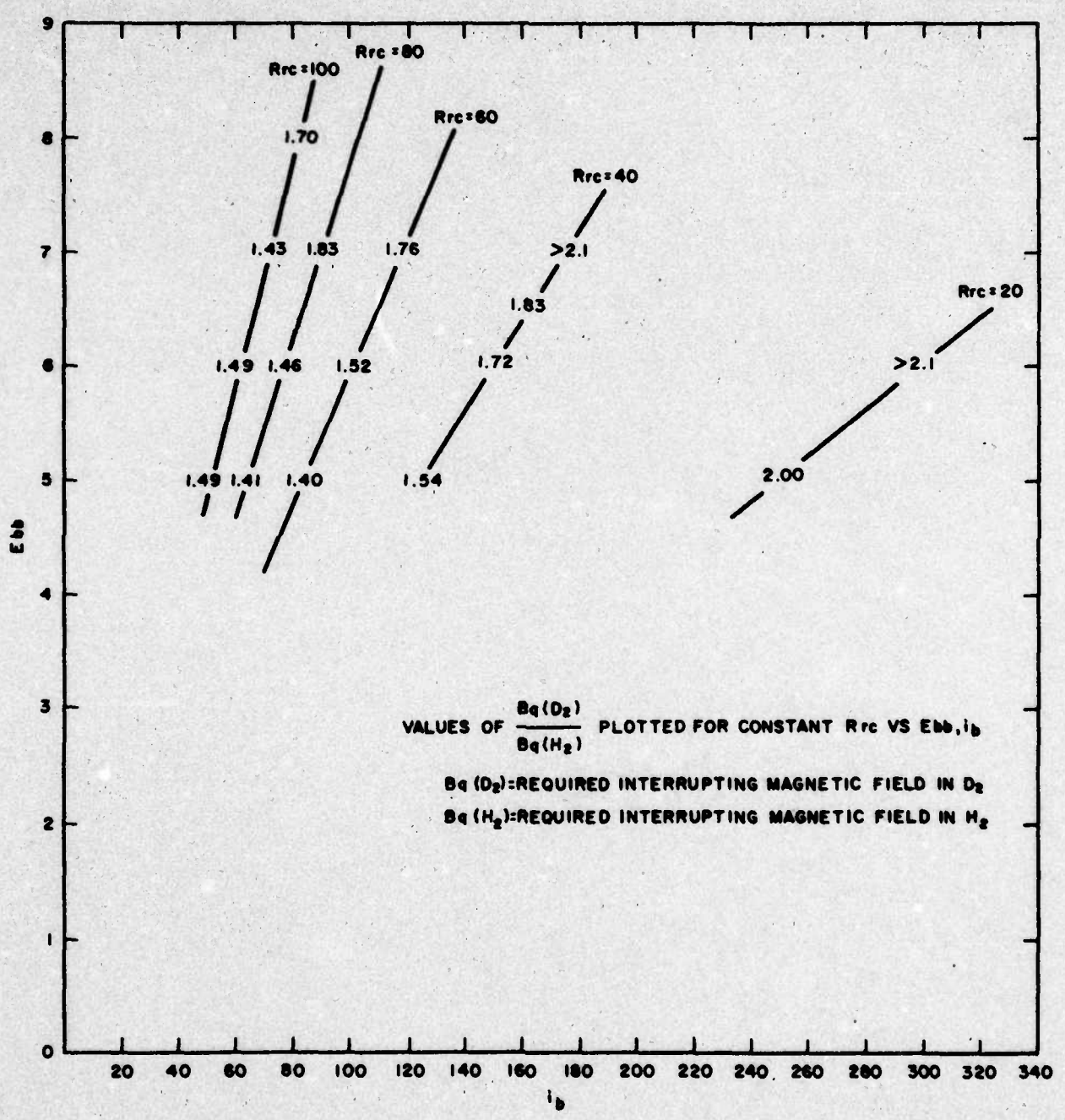

Figure 5. Interrupting magnetic field in deuterium vs. hydrogen as a function of Ebb, ib for RSI 004.

RSI 005 arced consistently at fairly low voltages between the glass envelope and the ceramic washers. An attempt to alleviate this problem by shrinking the glass onto a portion of the ceramic washer surface was not successful, because the glass fractured due to the difference in thermal expansion rates between glass and ceramic. Repair of the tube was not considered worthwhile, and an examination was made of the damage sustained by the ceramic washers.

Most of the damage to the ceramic occurred on the side of the washers facing the cathode, suggesting that erosion was caused by electron bombardment of the surface. The length of apparent plasma penetration into the washer to washer gap is also significant, since the 1 - 1.5 millimeter penetration depth (as determined from the extent of surface damage) into the plasma chute indicates an increase in the total discharge length by a maximum factor of only 1.7, as shown in Figure 6. The mechanism of improvement of tube interruption probably stems, therefore, from direct electron surface energy losses rather than from a radical bending and folding of a narrowed discharge column.

Also apparent from a visual observation of the washers was a difference in the degree of erosion depending upon location in the interaction tube. Washers near the cathode end suffered a greater amount of "burning" than those near the anode end. In addition, the erosion near the cathode end was more diffuse, from one to several millimeters wide, whereas the anode end washers revealed "burning" to but one millimeter in width. Possible explanations for this behavior include longitudinal plasma density gradients, a nonlinear electric field distribution, a gas pressure gradient, high energy electron beaming, or a shift from a diffuse to a constricted discharge caused by interaction with the washer edges.

The ceramic washers removed from the tube were eroded radially for approximately 1 mm from the central plasma bore, in the expected $\vec{I} \times \vec{B}$ direction of magnetic force. An SEM (Scanning Electron-Microprobe) X-ray

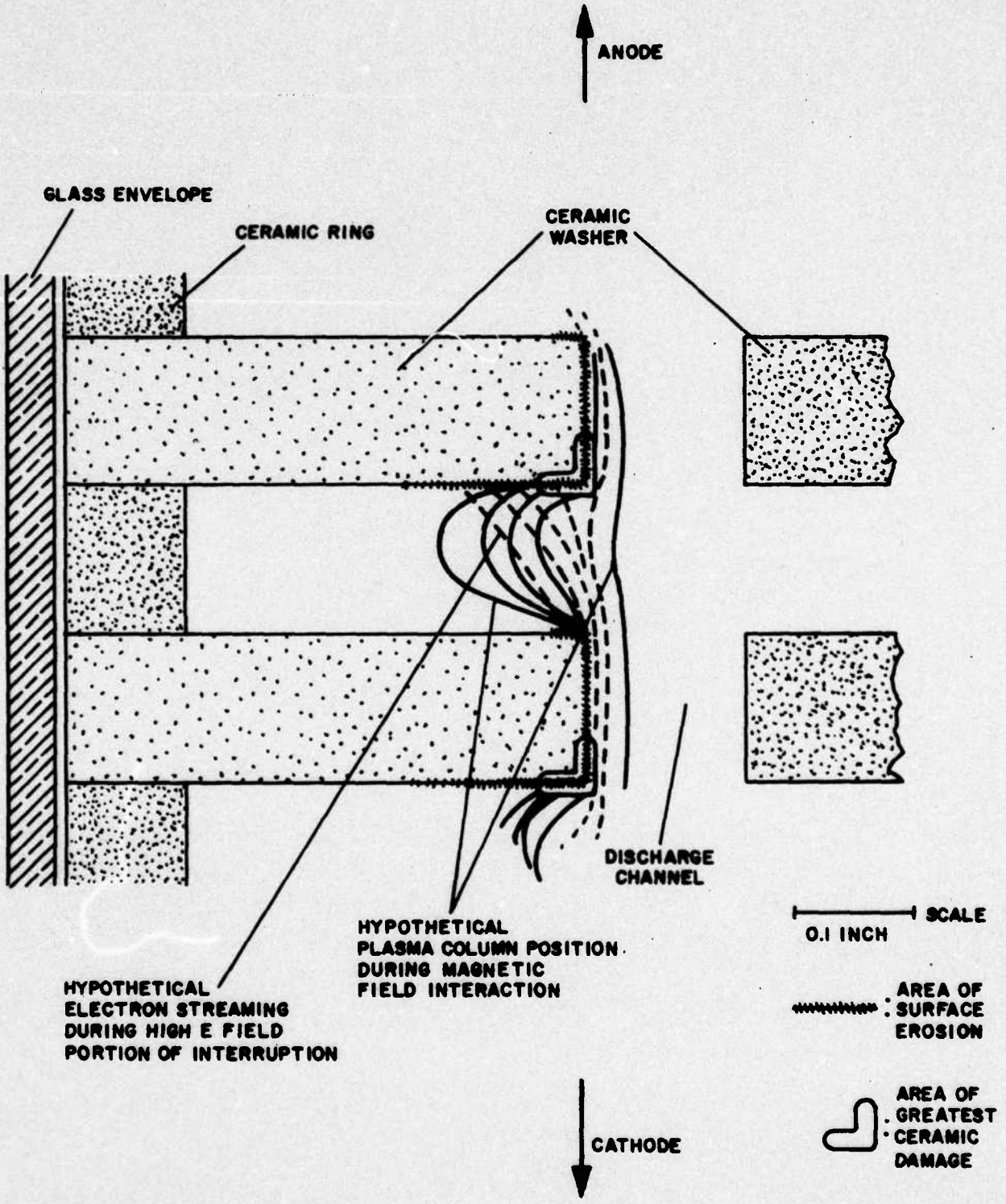

Figure 6. RSI 005 during magnetic field interaction.

analysis was performed on the eroded surface (Figures 7, 8), looking particularly for possible electrode metal contamination. The analytical report indicated weak concentrations of Fe, Ni, Ta, and Mn in only a small portion of surface area. Most of the surface damage appears to have been caused by wall heating by the hydrogen plasma.

The analysis was made in the magnesium to uranium mass range, using Ortec spectrum X-ray fluorescence detector equipment.

The concern, therefore, that large amounts of metal vapor might contaminate the plasma was unsubstantiated, probably due to the distance between the interaction region of high magnetic field strength and the glass-metal seals.

The RSI 005 was tested at an average voltage of 8 kV, at an average current of 160 amps. A power dissipation calculation can be made, utilizing the assumptions of: an average 10 μsec interruption time, an average penetration depth of 1 mm into the washer to washer gap, and an average discharge column width during interruption at the ceramic surfaces of 1 mm. The result indicates an average short time scale wall surface heating of about 900^{o}C, which suggests that ceramic erosion could be occurring during the higher power testing phase. At the peak power level, Ebb = 7.5 kV, ib = 375 amp, and the calculated surface temperature is approximately 2000^{o}C.

2.3 MAGNETIC FIELD PULSE SHAPING

Prevention of restriking of the fault discharge after current interruption is extremely important to the success of the RSI program. One proposal for restrike prevention is for the shaping of the magnetic field pulse to provide two functions. The first portion of the pulse would interrupt the discharge, with a short rise-time, high magnetic field. A second pulse would continue from the first, at a considerably lower level, to prevent restriking. It has been observed that the strength of the magnetic field after interruption had an effect upon restriking behavior, particularly in that allowing the magnetic

Figure 7. Surface damage to RSI 005 ceramic washer.

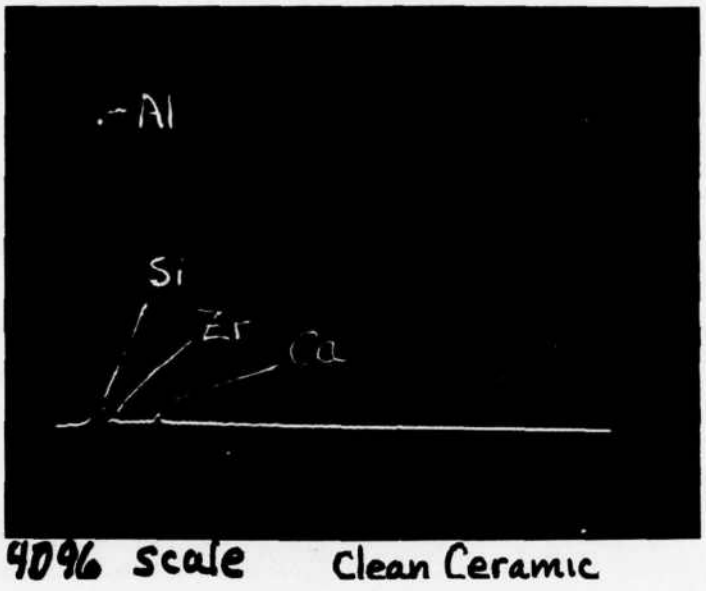

(a) Undamaged ceramic

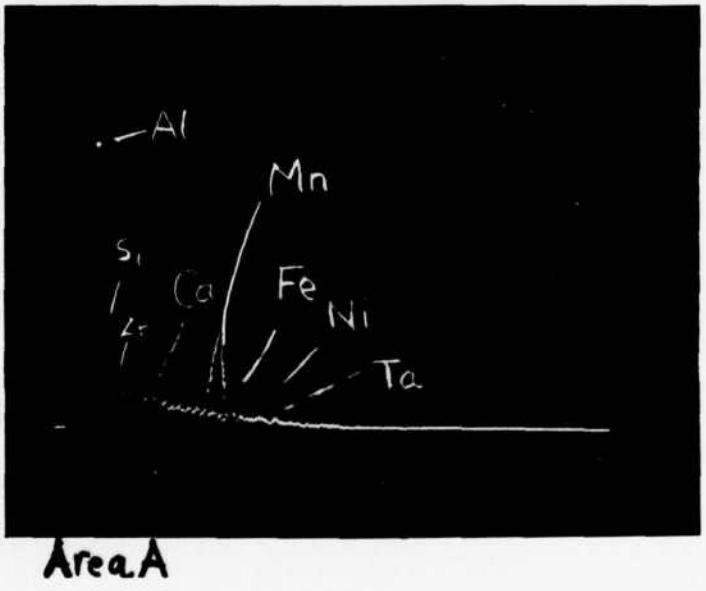

(b) Eroded surface (expanded scale)

Figure 8. SEM analysis of RSI 005 ceramic washer surface.

field to ring also allowed the current discharge to restrike at approximately the time that the field passed through zero. A pulse-shaping circuit as shown in Figure 9 was therefore devised for testing restrike prevention. The series thyratron was removed from the circuit, the RSI holdoff section being used to provide high voltage recovery.

Typical test results from this circuit are shown in Figure 10, where the deuterium-filled RSI 004 was under test, triggered directly with a 4-kV pulse. A typical magnet current is shown in Figure 10a. Figure 10b shows restrike prevention at 5.9 kV, at which point roughly 70% of all fault pulses are completely quenched (lower Ebb discharges are interrupted completely with progressively better consistency). Figure 10c shows a slightly different case, where restriking after several hundred microseconds was a problem. Different capacitor values were used in each case; the number of magnet turns was also adjusted. The restriking shown in Figure 10c, occurring at lower Ebb, takes place at approximately the same field levels as that shown in Figure 10b, but with a longer period of delay, and a greater variability of delay time. The apparent increase of restriking at lower Ebb is not understood.

For longer time scale restrike prevention, the circuit shown in Figure 11 was devised, but to date has failed to yield a satisfactory pulse waveform. A difficulty with the coupling of short and long magnet coils, which necessarily requires coils of a few and many turns, is that the high dB/dt induced in the magnet by the fast coil produces dangerously high voltages in the many-turn coil.

Further study must be given to the use of grid bias and other external circuitry, as well as to new magnet pulse-shaping techniques, to improve restrike prevention. H_2 must be used as a fill gas, and further examination must be made of anode-grid voltage waveforms during restriking.

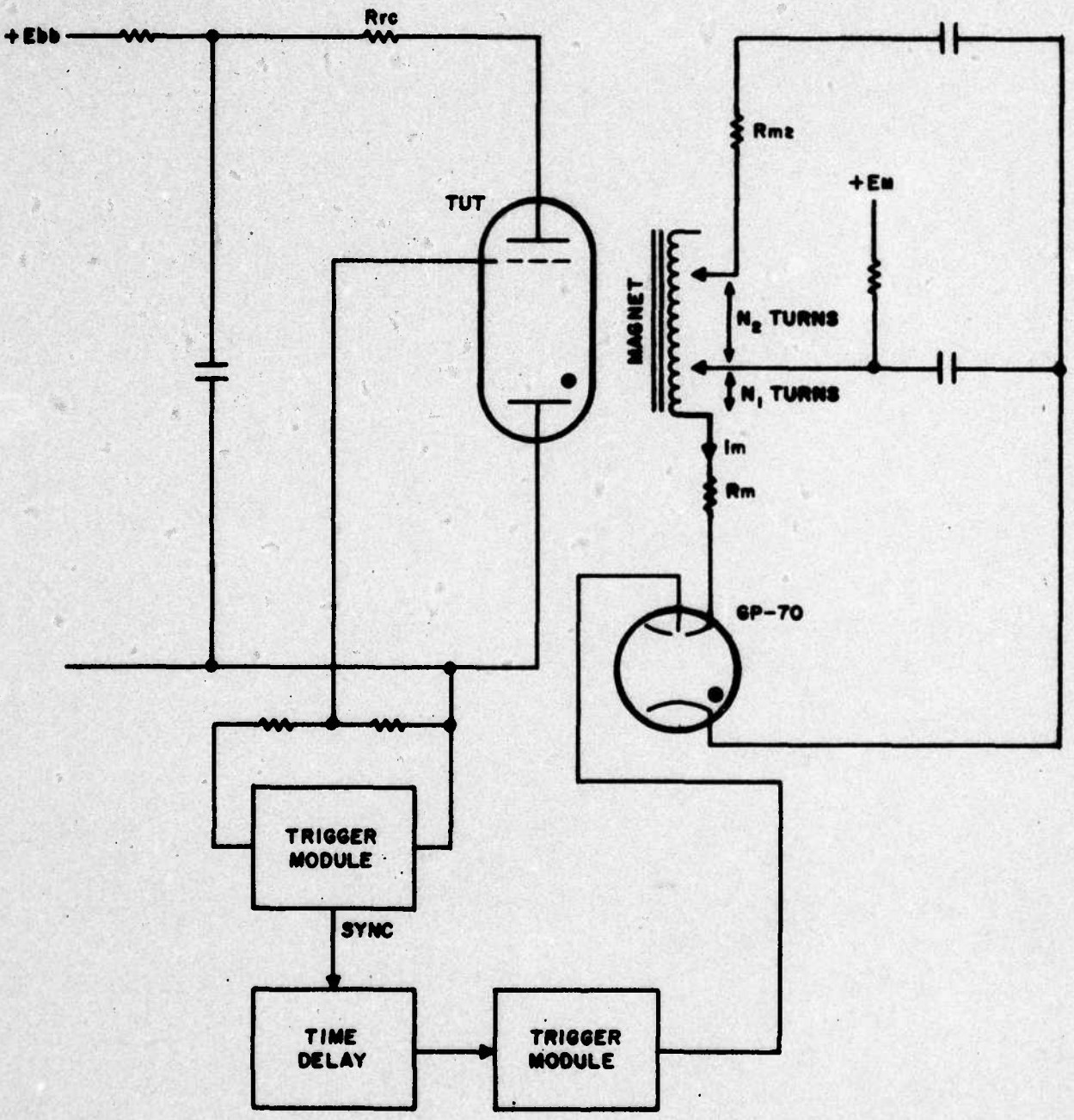

Figure 9. Magnetic field shaping test circuit.

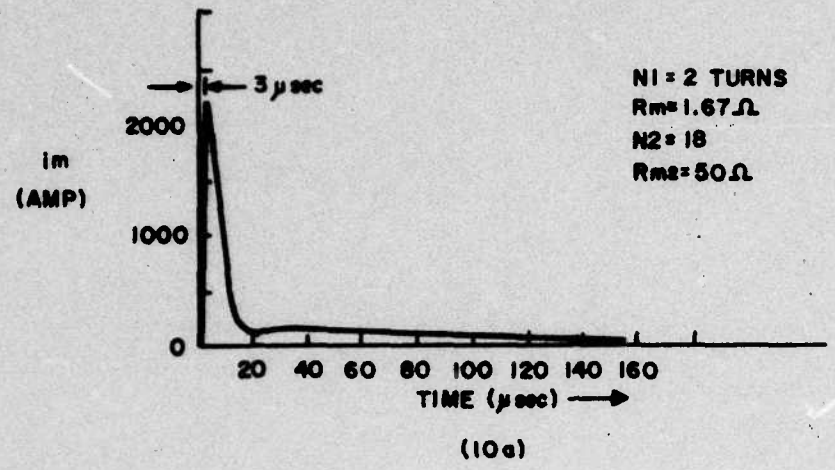

(10a)

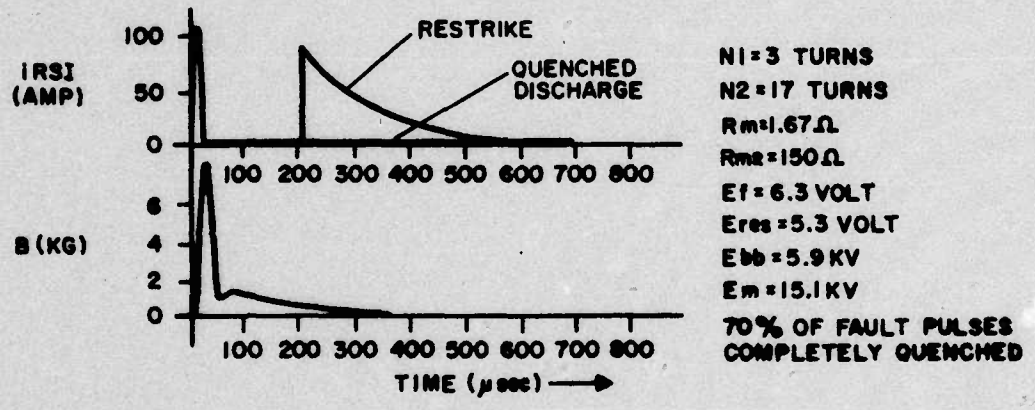

(10b)

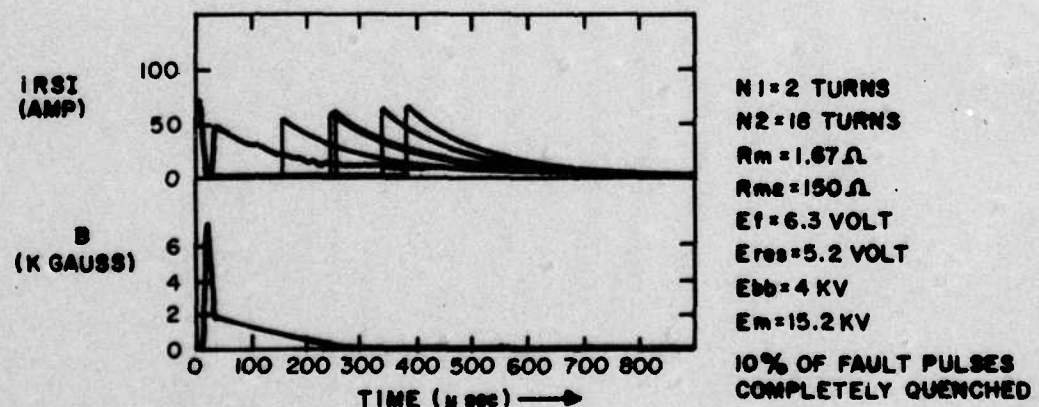

(10c)

Figure 10. Fault discharge restriking in D_2-filled RSI 004.

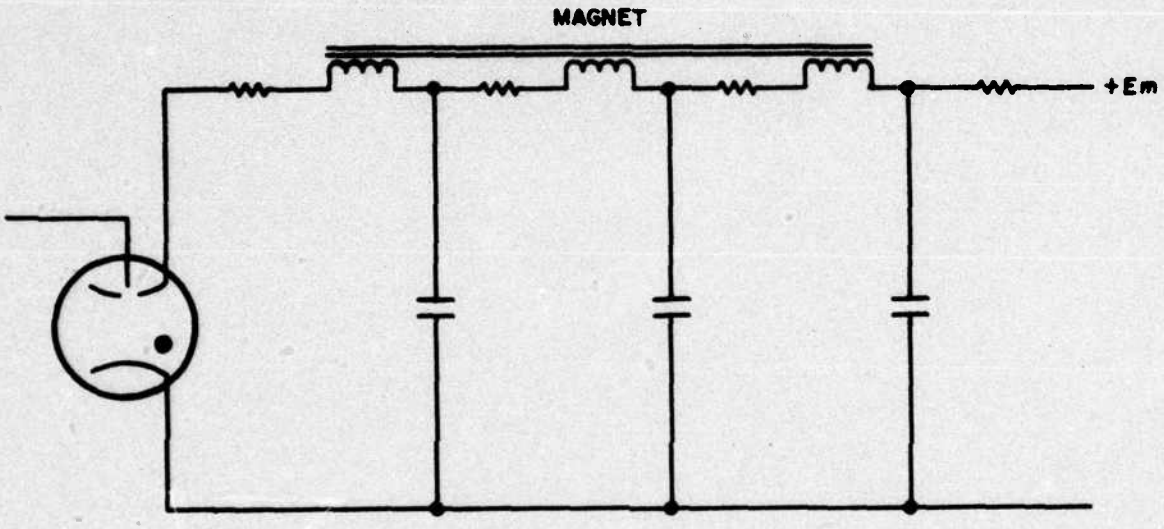

Figure 11. Alternate field shaping circuit.

2.4 *MAGNETIC FIELD RISE TIME TEST*

In conjunction with the field shaping study, the effect of the speed of the magnetic field rise time on the required interrupting magnetic field was observed. The magnet circuit shown in Figure 12a was used, where N and Rm were varied to produce a series of near critically damped magnet current pulses, with varying rise times. Results are shown in Figure 12b, and they seem to indicate an optimum rise time of 10 microseconds. These data should be looked at with a degree of caution, however, since: (1) inductances elsewhere in the circuit become comparable to the magnet inductance at low values of N, so that stray magnetic fields become an important factor; and (2) each data point represents a different waveshape corresponding to a slightly different degree of overdamping.

2.5 SERIES TUBE POWER DISSIPATION

The purpose of the RSI tube is to prevent damage from occurring in the travelling wave tube which will operate in series with the RSI. To minimize damage in the TWT, power dissipation should be kept to a minimum. This power dissipation, during the fault conduction period, can effectively be taken as equal to $\int VI\,dt$ for the period in which the fault current is being carried. This value is essentially equal to $V \int Idt = VQ$, where Q equals the total charge transferred during this interval. This assumes an arc occurs in the travelling wave tube, with an arc voltage between 10 and 100 volts. To keep the total dissipation under 1 joule, Q should be less than 0.01 coulomb. Q may be regarded as a useful figure of merit for the RSI, since this parameter is proportional to the amount of energy dissipated in the microwave tube.

Our present tubes are capable of switching off in a period of roughly 10 microseconds. The $\int Idt$ is somewhat less than $\frac{1}{2}\, ib\,\Delta t$, which for a peak current of 300 amps yields Q = 0.0015 coulomb, which would indicate an energy dissipation of 0.15 joule in the faulted TWT. This assumes that the RSI magnet is switched on immediately (less than 1 microsecond) after the

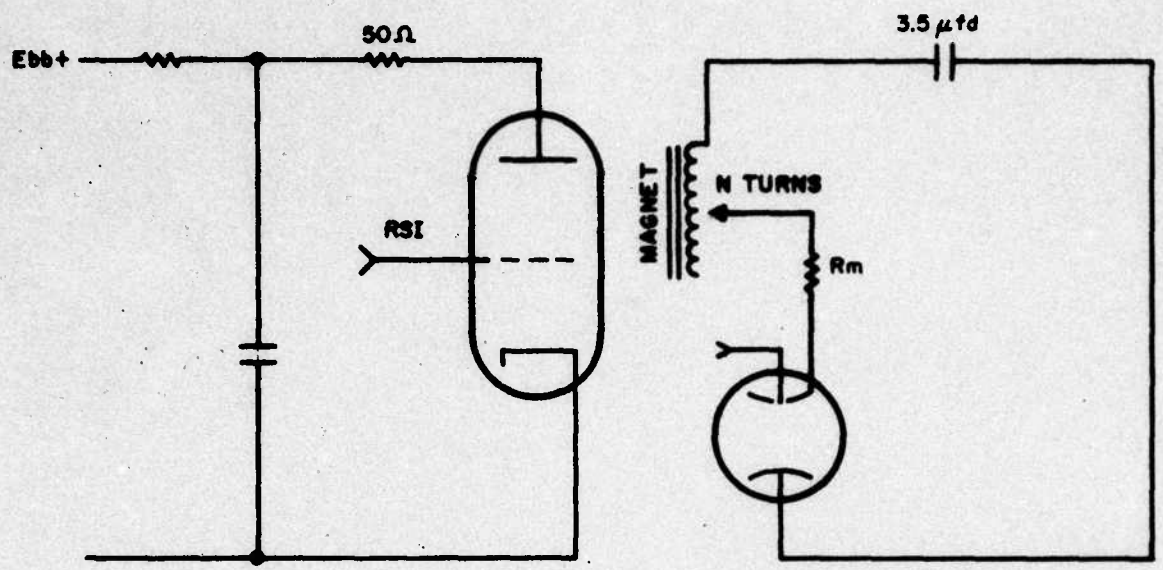

(12a)

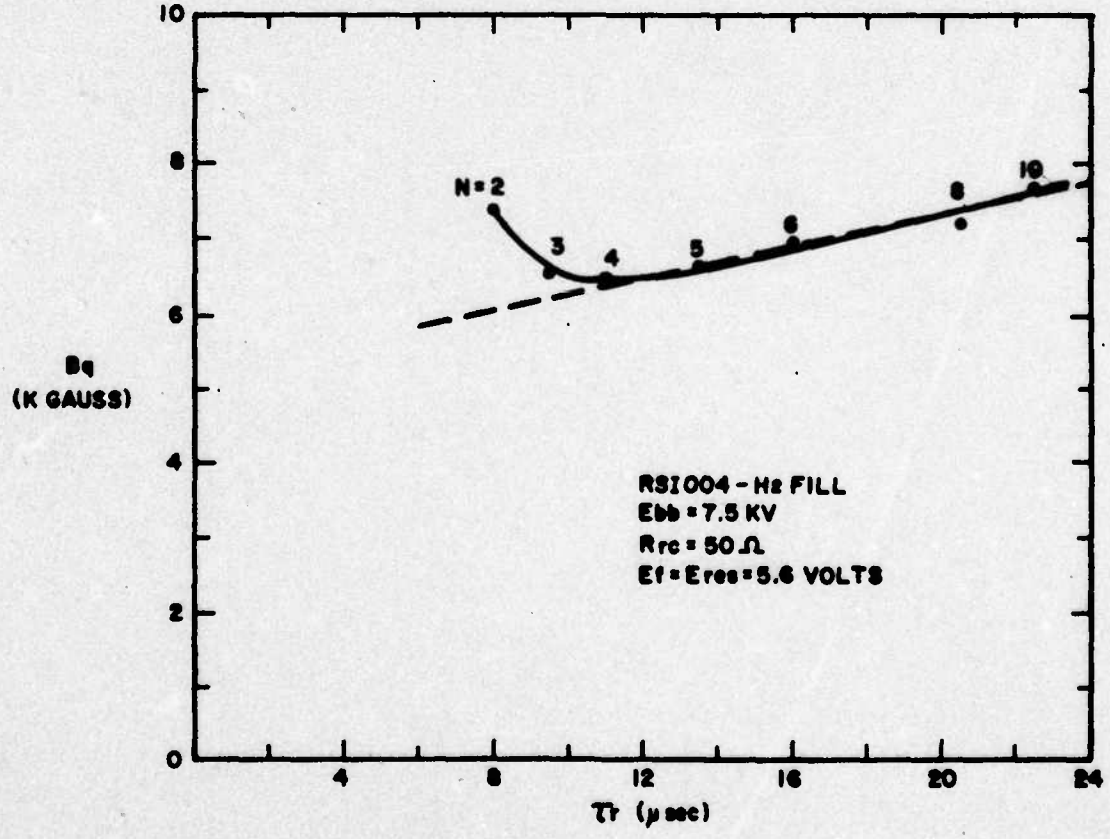

(12b)

Figure 12. Interrupting magnetic field vs. magnet pulse rise time.

fault current begins. Even if an extreme delay of 5 microseconds is assumed for firing the RSI, the total Q switched would only double, so that series tube power dissipation would still be only 0.3 joule.

It is also possible to reduce these numbers still further by decreasing the magnetic field rise time. A 5-microsecond field rise time is possible; combined with a realistic 3-microsecond firing delay, total charge transferred, Q, would equal 0.00165 coulomb. The problem that develops here is that high voltages are induced in the long pulse magnet by the fast rise time of the interrupting field. These can be overcome at the expense of high capacitor storage energy discharged through a magnet coil with a moderate number of turns.

2.6 TUBES UNDER CONSTRUCTION

Several tubes which were planned earlier have been combined into a single entity, with separable cathode and interaction region – anode region sections. A standard HY-11 cathode has been mounted on a 1.5-inch I.D. Varian flange. Several anode sections are planned which will be mounted on gasket adapters and bolted to the cathode section. This design provides for ease of assembly of several individual tubes, cost and assembly time reduction, standardization of cathode behavior, and provision for direct pressure monitoring, with a Hastings gauge directly mounted to the cathode assembly.

Three anode interaction sections are presently being built. Test pieces had been tried to determine reliable methods of high temperature sealing to the MACOR machinable ceramic anode sections. Although the test pieces provided good sealing, some difficulty was encountered when the interaction sections were used, for several reasons. A MACOR metallization process was tried, using Ag/Pt with a BT silver-copper vacuum braze to expansion matched Fe/Ni, with the result that the metallization and the brazing material intermixed and beaded up in one of two operations, suggesting the need for critical temperature control. Titanium hydride bonding was tried and provided apparently strong seals, but fractured the ceramic. The problem

appears to be expansion differences over a range of temperatures up to the brazing temperature. A solution may be to weaken (make thinner) metal anodes and connectors. Corning 7575 glass frit does an apparently adequate sealing job, but suggests sealing at a 450°C temperature, which will reduce the allowable bakeout temperature, but may offer the best solution to the problem. One difficulty with frit seals is an apparent penetration of Fe-Ni into the frit, reducing the strength of the seal.

2.7 ANALYSIS OF A POSITIVE COLUMN IN A TRANSVERSE MAGNETIC FIELD

In the interests of better defining the physical mechanisms of current interruption in an RSI crossed-field type device, a theoretical analysis was undertaken of the positive column of a gaseous discharge with a transverse applied magnetic field.

Professor Peter Politzer of the Department of Nuclear Engineering at MIT performed the following examination of a crossed-field discharge in a rectangular discharge column with coordinates and field directions as shown in Figure 13. MKS units are used throughout. The following assumptions are made.

1) The plasma is a weakly ionized hydrogen plasma with electron temperature less than 5 eV.

2) All parameters are independent of the longitudinal direction ($\frac{\partial}{\partial z} = 0$).

3) The rise time of the magnetic field is sufficiently slow, compared with plasma time constants, so that the plasma can be considered to be in a steady state ($\frac{\partial}{\partial t} = 0$).

4) Lower-order electron and ion temperature gradient and mass terms are neglected.

5) Charge neutrality ($n_i = n_e$) exists throughout the plasma.

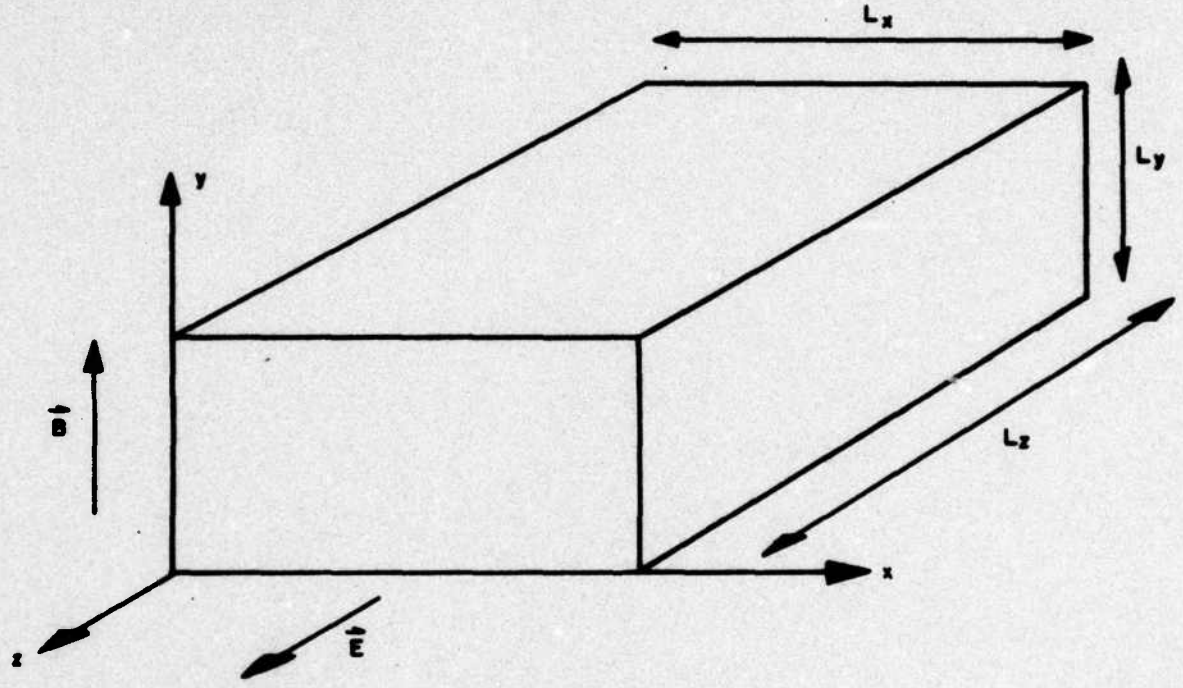

Figure 13. Geometry for positive column analysis.

Then, solution of the momentum conservation equations:

$$m_e n_e \frac{\partial \vec{V}_e}{\partial t} + m_e n_e \vec{V}_e \cdot \nabla \vec{V}_e = - \vec{\nabla}(n_e T_e) - n_e e \vec{E} - n_e e \vec{V}_e \times \vec{B} - \frac{n_e e}{\mu_e} \vec{V}_e$$

$$m_i n_i \frac{\partial \vec{V}_i}{\partial t} + m_i n_i \vec{V}_i \cdot \nabla \vec{V}_i = - \vec{\nabla}(n_i T_i) + n_i Ze\vec{E} + n_i Ze \vec{V}_i \times \vec{B} - \frac{n_i Ze}{\mu_i} \vec{V}_i$$

yields, for the current density $\vec{J} = n_e e (\vec{V}_i - \vec{V}_e)$:

$$J_x = \frac{n_e e}{(1 + \mu_e^2 B^2)(1 + \mu_i^2 B^2)} \left[E_x (\mu_e + \mu_i)(1 + \mu_e \mu_i B^2) + E_z (\mu_e^2 - \mu_i^2) B + \frac{k T_e}{e} \mu_e \frac{1}{n_e} \frac{\partial n_e}{\partial x} (1 + \mu_i^2 B^2 - \frac{\mu_i}{\mu_e} \frac{T_i}{T_e} - \mu_e \mu_i B^2 \frac{T_i}{T_e}) \right]$$

$$J_y = n_e e \left[E_y (\mu_e + \mu_i) + \frac{k T_e}{e} \mu_e \frac{1}{n_e} \frac{\partial n_e}{\partial y} (1 - \frac{\mu_i}{\mu_e} \frac{T_i}{T_e}) \right]$$

$$J_z = \frac{n_e e}{(1+\mu_e^2 B^2)(1+\mu_i^2 B^2)}\left[-E_x(\mu_e^2-\mu_i^2)B\right.$$

$$+E_z(\mu_e+\mu_i)(1+\mu_e\mu_i B^2) - \frac{kT_e}{e}B\frac{1}{n_e}\frac{\partial n_e}{\partial x}(\mu_e^2+\mu_i^2\frac{T_i}{T_e}$$

$$\left.+\mu_e^2\mu_i^2 B^2(1+\frac{T_i}{T_e}))\right]$$

Let

$f_i = f_i(T_e, n_o)$ = ionization rate per electron.

In the steady state:

$$\vec{\nabla}\cdot\vec{J} = 0;$$

$$\nabla\cdot(n_e\vec{V}_e) = n_e f_i .$$

These two equations provide solutions for the two unknowns $n_e(x, y)$, $E(x, y)$, with the boundary conditions at the walls:

$$\vec{J} = 0;$$

$$n_e = 0.$$

An analytical solution to the above equations is not attainable, which suggests further simplification. For both B = 0 and B very large, the above equations require that $J_x = J_y = 0$. Furthermore, J_x, J_y are not zero only when circulatory currents develop in the transverse direction in the plasma. Because the principal electrically and magnetically induced plasma motion occurs in the longitudinal planes, any transverse circulatory current must be necessarily second-order, and can be neglected. This is particularly appropriate since the plasma time constants are short compared to the B time, and since this represents the steady state assumption previously made.

Setting $J_x = J_y = 0$, therefore, yields equations for E_x and E_y as functions of n_e and E_z. From these, a solution for J_z can be determined:

$$J_z = \frac{n_e(x,y)e}{1+\mu_e \mu_i B^2}\left[E_z(\mu_e+\mu_i) - \frac{k T_e}{e}\frac{1}{n_e}\frac{\partial n_e}{\partial x}\mu_e \mu_i B\left(1+\frac{T_i}{T_e}\right)\right]$$

as well as for the transverse electron velocities. These velocities, substituted into the equation $\vec{\nabla}\cdot(n_e \vec{V}_e) = f_i n_e$ yield:

$$\frac{\partial^2 n_e}{\partial x^2} + (1+\mu_e \mu_i B^2)\frac{\partial^2 n_e}{dy^2} + \frac{(\mu_e+\mu_i) Be E_z}{k(T_e+T_i)}\frac{\partial n_e}{\partial x}$$

$$+ f_i \frac{e}{k(T_e+T_i)}\frac{\mu_e+\mu_i}{\mu_e \mu_i}(1+\mu_e \mu_i B^2) n_e = 0$$

Assuming that the y dependence for n_e is proportional to $\sin\left(\frac{\pi}{L_y} y\right)$ yields:

$$\frac{\partial^2 n_e}{\partial x^2} + \alpha \frac{\partial n_e}{\partial x} + \beta n_e = 0$$

where

$$\alpha = (\mu_e+\mu_i) B \frac{e}{k(T_e+T_i)} E_z$$

$$\beta = \left[f_i \frac{e}{k(T_e+T_i)}\frac{\mu_e+\mu_i}{\mu_e \mu_i} - \frac{\pi^2}{L_y^2}\right](1+\mu_e \mu_i B^2)$$

This result contains the assumption that

$$\frac{\nu_i}{D} > \frac{1}{\Lambda^2},$$

or that the electron ionization be greater than the electron diffusion loss.

Boundary conditions of the form $n_e(0) = n_e(L_x) = 0$ define the solutions to the differential equation in n_e. For $n_e(0) = 0$, and for

$$\beta - \frac{\alpha^2}{4} < 0,$$

the solution for n_e is a hyperbolic sine function which cannot meet the second boundary condition. Therefore, for $\beta < \frac{\alpha^2}{4}$, no discharge can exist, and

$$\beta - \frac{\alpha^2}{4} > 0$$

represents the breakdown condition for the plasma, and the solution for n_e is:

$$n_e = n_{eo}\, e^{-\frac{\alpha}{2}x} \sin\sqrt{\beta - \frac{\alpha^2}{4}}\, x$$

and the electron ionization condition must accept the scale length $\Lambda_{eff} \simeq \frac{2}{\alpha}$. Applying the boundary condition gives

$$\beta - \frac{\alpha^2}{4} = \left(\frac{\pi}{L_x}\right)^2$$

and

$$n_e = n_{eo}\, e^{-\frac{\alpha}{2}x} \sin\frac{\pi x}{L_x}$$

where the electron density profile appears as in Figure 14, and the electron density maximum occurs at

$$x = x_* = \frac{L_x}{\pi} \tan^{-1}\left(\frac{2\pi}{\alpha L_x}\right)$$

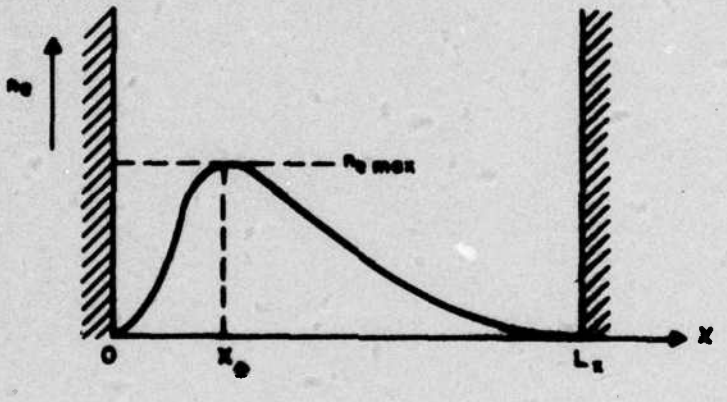

Figure 14. Solution form for electron density vs. x for a positive column in a transverse magnetic field.

The peak electron density and average electron density are readily determined, and are seen to reduce to the standard positive column for $B = 0$.

Integrating J_z over the cross-section gives the total current:

$$I = \frac{L_x L_y \mu_e n_{eo} e E_z \frac{2}{\pi^2} \left(1 + e^{-\left(\frac{\alpha L_x}{2}\right)}\right)}{\left[(1 + \mu_e \mu_i B^2)\left(1 + \left(\frac{\alpha L_x}{2\pi}\right)^2\right)\right]}$$

A final examination of energy balance in the plasma yields the equation:

$$\left(\frac{k T_e}{e}\right)^2 = \frac{1}{6f} \frac{L_e^2 E_z^2}{1 + \mu_e \mu_i B^2} \left[1 + \frac{\mu_i}{\mu_e} - \frac{k T_e}{e} \frac{\mu_i B}{E_z} \frac{1}{n_e} \frac{\partial n_e}{\partial x} \left(1 + \frac{T_i}{T_e}\right)\right]$$

As long as the last term in the brackets is small, a simple expression is derived for $T_e = T_e (E_z)$. Should this not be the case, the calculations must be repeated, including ∇T_e terms.

The foregoing theory has been further considered to compare its results with the available experimental data.

For our conditions, the reduced discharge radius, x_*, can be approximated with the use of

$$\tan^{-1}\left(\frac{2\pi}{\alpha L_x}\right) = \frac{2\pi}{\alpha L_x},$$

for $\alpha L_x \gg 1$.

With $\alpha \cong \mu_e \frac{BE_z}{\left(\frac{KT_e}{e}\right)}$, and $\mu_e\ (m^2/v\cdot sec) \cong \frac{49}{p_o(torr)} \frac{1}{\sqrt{\frac{KT_e}{e}}}$

then

$$x_* \cong \frac{2}{\alpha} = \frac{T_e^{\frac{3}{2}}\ p_o}{25\ B\ E_z}\ (m, eV, torr, T, V/m)$$

or, at $p_o = 0.3$ torr, $T_e = 4$ eV:

$$x_*(cm) = \frac{0.14\ T_e^{\frac{3}{2}}}{B(Kgauss)\ E(volt/cm)} = \frac{1.1}{B\ E}$$

To determine the predicted interrupting field, the voltage drop in a channel of radius x_* should be made equivalent to the applied electric field; that is, the magnetic field should be seen as a mechanism of constricting the plasma column, and thereby increasing the electric field in the plasma to the point at which the electric potential can no longer support the discharge energy losses.

Data for E/p versus rp at very low rp, however, are not available, and it becomes necessary to extrapolate from data four orders of magnitude higher, as shown in Figure 15.

Experimental data at $0.1 < rp < 10$ suggest that $\frac{E}{p} \cong 16\ (rp)^{-0.5}$, under 20-amp pulsed discharge conditions. An extrapolation of this formula to 300-amp pulses can be made from Figure 3a data, suggesting that $\frac{E}{p} \cong 12\ (rp)^{-0.5}$, or that

$$E \cong 12\sqrt{\frac{p}{r}}$$

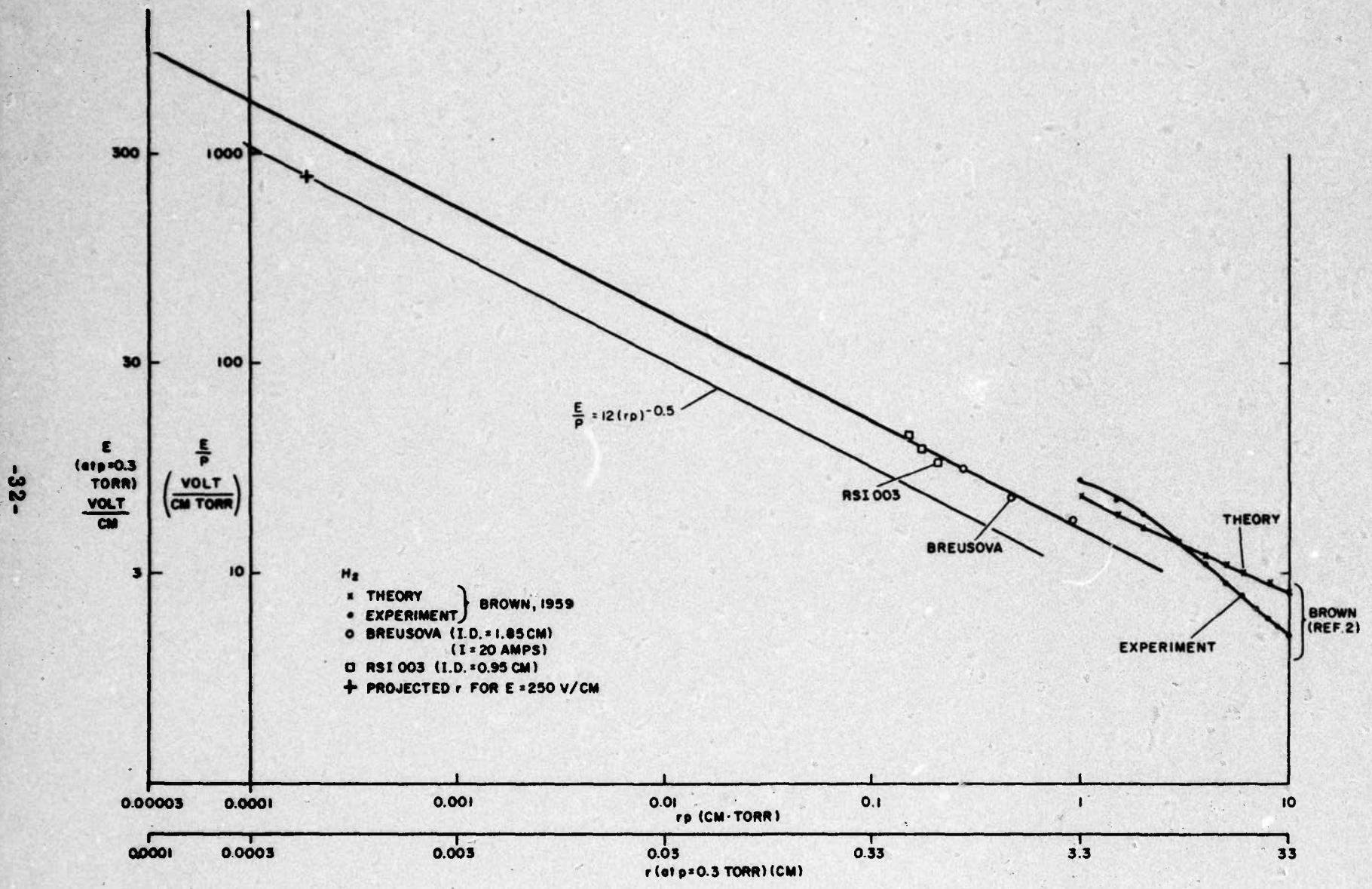

Figure 15. E/p vs. rp: an extrapolation of e_{td}.

Since $x_* \equiv r$, we find that at B = Bq:

$$Bq = \frac{0.14\ T_e^{\frac{3}{2}}}{E} \cdot \frac{E^2}{144p} \cong 0.001 \frac{T_e^{\frac{3}{2}} E}{p} \quad \text{(Kgauss, eV, volt/cm, torr)}$$

at $p_o = 0.3$ torr, $T_e = 4$ eV we predict that Bq = 0.025 E.

These results can be compared with our experimental observations. The RSI 003 tube was observed at Ebb = 15 kV, ib = 300 amps, L = 60 cm, p = 0.30 torr, and E = 250 volt/cm to require an interrupting field, Bq, equal to 5 kilogauss, while the predicted interrupting field is 6.25 kilogauss. The RSI 004 tube (at Ebb = 10 kV, ib = 200 amps, L = 16 cm, p = 0.35 torr, and E = 625 volt/cm) required a field of 9.5 kilogauss, while the predicted value equals 13.6 kilogauss.

Considering the number of approximations made in our calculations, the agreement between theory and experiment is remarkably good, although the predicted dependencies of $Bq \propto \frac{E}{p} T_e^{\frac{3}{2}}$ do not directly agree with the empirical formula of $Bq \propto Ebb^{1.25} L^{-0.75} ib^{0.25} p^{+1}$. This deviation may be explainable in that the electron temperature of a positive column is a nonanalytical inverse function of rp, which fact establishes a better (but not analytically derivable) correlation between the two expressions.

A further test of the theory can be made by comparing the predicted values for x_* with the width of the surface damage to the RSI discharge channel walls, and with the image converter observations of discharge column light intensity during interruption. Figure 16 depicts the cross-sectional geometry of the RSI 003 discharge channel with an approximate contour (presumed) for the plasma column during magnetic constriction. Wall damage along the arc $\overset{\frown}{AC}$ can be used to provide an estimate of the average discharge diameter (a) during the energy dissipative portion of the discharge (for a<<b, $a \cong R_1 - \sqrt{(R_1)^2 - (\overset{\frown}{BC})^2}$).

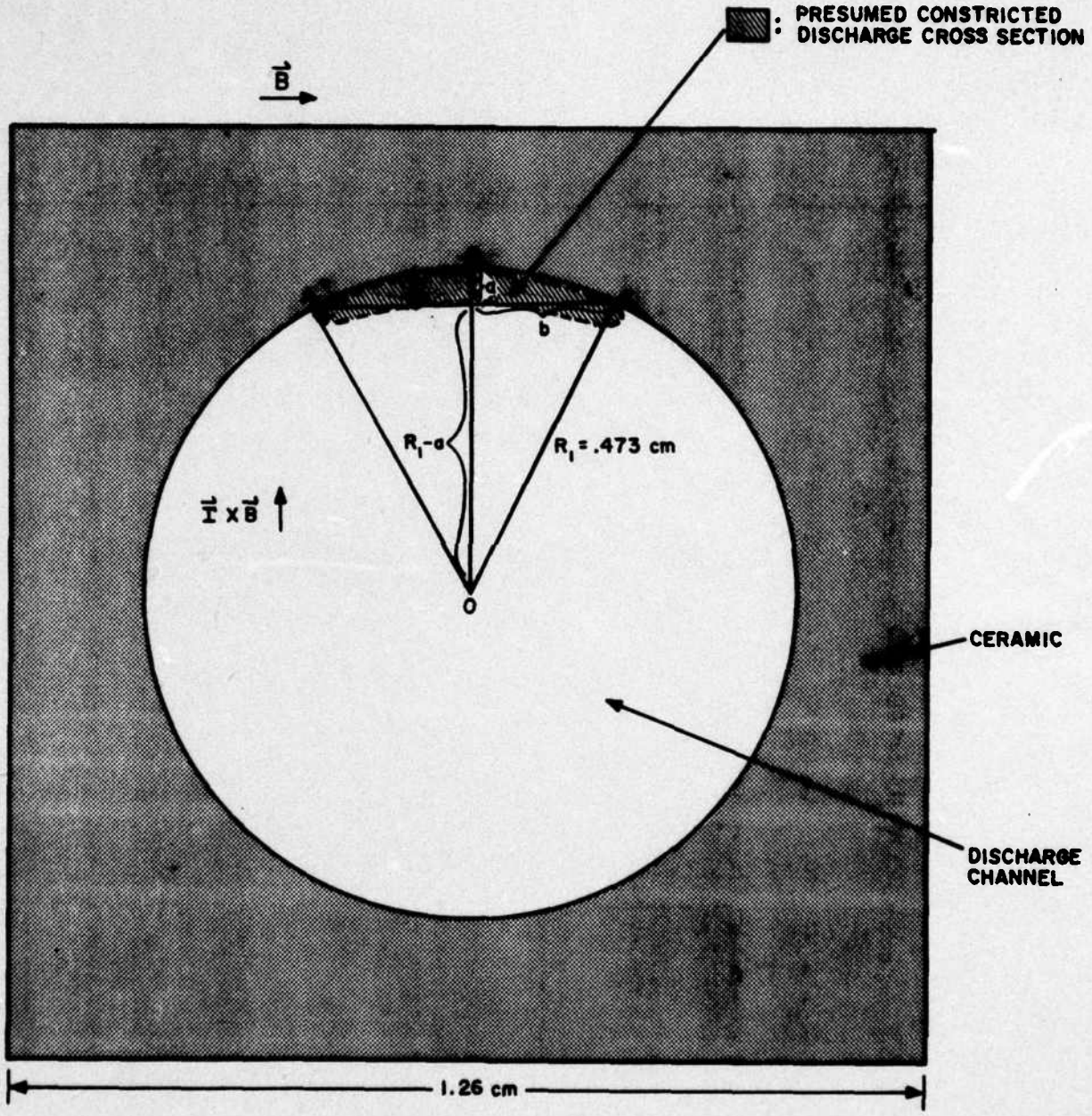

Figure 16. RSI 003 tube and discharge cross-section dimensions.

For RSI 003 (R_1 = 4.7 mm), slight wall damage occurred along an arc $\widehat{AC}$ of approximately 2 mm, which indicates an $x_* = a/2 \cong 0.05$ mm. At Bq = 6.25 kilogauss, E = 250 volt/cm, our theory predicts that $x_* = 0.07$ mm. Maximum energy dissipation to the wall surface will occur at a point in time midway through interruption, at which time $B \cong \frac{1}{2}$ Bq, $E \cong \frac{1}{2}$ Ebb, $iRSI \cong \frac{1}{2}$ ib, and $x_* = 0.03$ mm. This latter value approaches the theoretical prediction.

For RSI 004 (R_1 = 3.5 mm), heavy wall damage occurred along $\widehat{AC}$ = 2 mm, indicating an $x_* = a/2 = 0.08$ mm. Our theory predicts an $x_* = 0.002$ mm at Bq = 9.5 kilogauss, E = 625 volt/cm, or $x_* = 0.008$ mm at maximum power. Definite fine structure is observable in the wall damage to this tube at $\widehat{AC} = 0.13$ mm and 0.5 mm, corresponding to $x_* = 0.005$ mm and 0.018 mm, which range close to the predicted x_*. Since both RSI 003 and RSI 004 were operated at lower values of Ebb and Bq, some wider damage tracking would be expected by theory. Therefore, damage assessment observations agree with theoretical calculations within experimental limits.

Image converter observations taken earlier are not as accurate an assessment of discharge diameters as are wall damage assessments due to: (1) light scattering by the channel walls, (2) thermal retention by the wall surfaces during the interrupted pulse, (3) neutral hydrogen afterglows, and (4) the limited quality of the photographs obtained. Results confirm the qualitative nature of the constriction of the discharge during interruption.

An increase in electron temperature during interruption has not directly been taken into consideration in this analysis, and could pose the problem of considerably increasing the predicted values for Bq and x_*. As previously mentioned, positive column theory predicts that T_e increases with decreasing r. The narrow diameter crossed-field discharge under study here may diverge from this point of theory due to the greater cooling action of the channel wall on impinging electrons. Furthermore, relatively slow secondary electrons may comprise a substantial portion of the discharge current, thus lowering the average electron temperature.

Factors of electron temperature, plasma energy loss mechanisms, and the nature of the plasma-wall sheath and its effects upon the constricted discharge require further study. Analysis of these factors may provide a better solution to the nonlinear dependence of Bq on Ebb. In addition, an examination of gas depletion effects may clarify the fourth root nonlinearities of Bq with ib and L.

2.8 FINAL TUBE DESIGN CONSIDERATIONS

Although the plasma chute machinable ceramic tubes have not been completed or tested, it is important to begin the design of the final tubes for the contract. The decision has been made to make use of the plasma chute interaction design, based on its performance in the RSI 005, and on the ultimate need for higher voltage interrupters.

Since the final tubes are still experimental, further decision was made to take advantage of the tube quantity required by exploring a diversity of interaction channel dimensions, as much as tube construction will allow. The interaction section design has been narrowed to a selection from four techniques for construction of ceramic forms, and will be soon finalized. Plasma chute designs again range from the 0.125-inch diameter bore lower limit through 0.375-inch maximum. The important second variable will be the bore of the plasma chutes.

Assuming a 50% reduction in the required magnetic field by the use of a plasma chute design (preliminary results indicated 67%), a 6-inch long, 0.375-inch bore chuted channel would require a 9.4 kgauss quenching field and would result in a 210-volt interaction region drop and a calculated 25-joule magnetic field. The range of final tubes will explore deviations centered at numbers comparable to these.

Standard cathode and anode sections will be adapted for use with these tubes, with cathodes somewhat larger than the previous experimental tubes, to allow for higher average current and longer tube life.

2.9 CONTINUING STUDIES

The following studies are presently underway:

1) Thyratron grid-quenching study using a single 0.080-inch diameter grid aperture. Previous work revealed a quenching effect in standard thyratron tubes when the grid aperture is made insufficiently large to accommodate a high current density discharge. This study will attempt to determine whether this effect can be controlled without arcing behavior for use as a fault-limiting switch.

2) A multi-fold S-shaped interaction tube is being constructed to perform two tests: to determine whether electric field distortion by the presence of dielectric material obstructing the principal electron beam path can aid in discharge interruption and restrike prevention, and to determine whether local electric field reversals (accomplished by an appropriate resistor network with terminals of thin metal placed at the inside folds of the discharge column) can accomplish the same objective.

3) Work is continuing to solve the MACOR-metal sealing problems, in order to test the plasma chute interruption geometries.

4) An interaction region with a graded longitudinal electric field is under design. The presence of the magnet core on either side of the discharge channel could be expected to substantially alter the high voltage electric field distribution, particularly to a point where high fields occur during interruption between the holdoff section and the top of the magnet core and between the base of the core and the cathode, rather than in the body of the interaction region. Use will be made of a resistive voltage dividing network with wire-wrap coupling to the RSI 004 or RSI 001 interaction region. A second tube is being considered composed of a multi-grid interaction channel with many wide aperture grids equally spaced longitudinally in the channel. A similar resistive network would be coupled to these grids.

5) RSI 006, with a 6-section, 0.25-inch interaction channel will be constructed, pending results from the grid-quenching study, which will determine the type of holdoff region to be used. This tube will be used to investigate interruption scaling to higher Ebb and ib.

3. EXPERIMENTAL MODIFICATIONS

The test circuit remains largely unchanged from previous reports, with the exception that greater use was made of RSI triggering without the series 7322 thyratron. A TM-11A trigger module with a resistive voltage divider was used to determine the triggering voltage requirements (3 - 3.5 kV) of the D_2-filled RSI 004.

A GP-70 spark gap was added to the magnet circuit, replacing the parallel GP-20B and the aging GP-46. The GP-70 operates over the entire range of 3 to 20 kV.

A Machlett ML-6544 high-vacuum power triode was added to the circuit to simulate operation of a traveling wave tube in series with the RSI. The Machlett tube was discovered to have an air leak requiring tube replacement. An ML-7845 75-kV power triode was purchased to replace the tube, but it has not yet been installed.

Modifications to the magnet circuit have already been discussed. New, lower inductance load resistors were purchased to improve magnet efficiency and rise time when using small N magnet coils.

4. DISCUSSION OF RESULTS AND CONCLUSIONS

Investigations during this period provided further information for RSI tube design and uncovered problem areas which must be examined more closely.

Use of deuterium or heavier fill gases has been rejected for their contribution toward higher required magnetic field energies.

Modified magnetic field pulse shapes have been shown to be effective in delaying restriking behavior, but the long apparent recovery times which have been observed require further examination.

Analysis of plasma chute design induced ceramic erosion showed that life expectancies of RSI tubes may be low compared with standard thyratrons, and may suggest a future design where the magnetic field direction is rotated relative to the discharge channel during life, or where $\int_{\text{fault}} e_{td} i_{RSI} dt$ is made a critical parameter.

A cursory examination shows that $\int_{\text{quench}} V_{arc}\, i\, dt$ power dissipation in an arcing series vacuum tube will be within safe energy limits, particularly if $\int_{\text{fault}} e_{td}\, i_{RSI} dt$ is minimized. More compact tube and magnet geometries can be expected to decrease present switching rise times and magnet energy losses.

The theoretical positive column analysis presents a formal mechanism for current extinction by a solution for a reduced discharge channel radius as a function of the interrupting magnetic field. This result concurs somewhat with experimental observations, but requires further comparison with experimental results.

5. REFERENCES

1. Breusova, L. N., "Longitudinal Potential Gradient in a Positive Column in H_2 and D_2," Soviet Physics – Technical Physics, Vol. 14, No. 6, Dec., 1969.

2. Brown, S. C., Basic Data of Plasma Physics, MIT – Technology Press, 1966, p. 292.

DISTRIBUTION LIST

12 Defense Documentation Center
ATTN: DDC-TCA
Cameron Station (Bldg 5)
Alexandria, VA 22314

1 Code R123, Tech Library
DCA Defense Comm Engrg Ctr
1860 Wiehle Ave
Reston, VA 22090

1 Defense Communications Agency
Technical Library Center
Code 205 (P.A. TOLOVI)
Washington, DC 20305

1 Office of Naval Research
Code 427
Arlington, VA 22217

1 Director
Naval Research Laboratory
ATTN: Code 2627
Washington, DC 20375

1 Commander
Naval Electronics Laboratory Center
ATTN: Library
San Diego, CA 92152

1 CDR, Naval Surface Weapons Center
White Oak Laboratory
ATTN: Library, Code WX-21
Silver Spring, MD 20910

1 Rome Air Development Center
ATTN: Documents Library (TILD)
Griffiss AFB, NY 13441

1 Hq, Air Force Systems Command
ATTN: DLCA
Andrews AFB
Washington, DC 20331

2 CDR, US Army Missile Command
Redstone Scientific Info Center
ATTN: Chief, Document Section
Redstone Arsenal, AL 35809

1 Commander
US Army Missile Command
ATTN: DRSMI-RE (Mr. Pittman)
Redstone Arsenal, AL 35809

3 Commandant
US Army Aviation Center
ATTN: ATZQ-D-MA
Fort Rucker, AL 36362

1 Director, Ballistic Missile Defense
Advanced Technology Center
ATTN: ATC-R, PO BOX 1500
Huntsville, AL 35807

1 Commander
HQ Fort Huachuca
ATTN: Technical Reference Div
Fort Huachuca, AZ 85613

2 Commander
US Army Electronic Proving Ground
ATTN: STEEP-MT
Fort Huachuca, AZ 85613

1 Commander
USASA Test & Evaluation Center
ATTN: IAO-CDR-T
Fort Huachuca, AZ 85613

1 Deputy for Science & Technology
Office, Assist Sec Army (R&D)
Washington, DC 20310

1 CDR, Harry Diamond Laboratories
ATTN: Library
2800 Powder Mill Road
Adelphi, MD 20783

1 Director
US Army Ballistic Research Labs
ATTN: DRXBR-LB
Aberdeen Proving Ground, MD 21005

1 Harry Diamond Laboratories, Dept of Army
ATTN: DRXDO-RCB (Dr. J. Nemarich)
2800 Powder Mill Road
Adelphi, MD 20783

1 Commander
US Army Tank-Automotive Command
ATTN: DRDTA-RH
Warren, MI 48090

1 CDR, US Army Aviation Systems Command
ATTN: DRSAV-G
PO Box 209
St. Louis, MO 63166

1 TRI-TAC Office
ATTN: CSS (Dr. Pritchard)
Fort Monmouth, NJ 07703

1 CDR, US Army Research Office
ATTN: DRXRO-IP
PO Box 12211
Research Triangle Park, NC 27709

1 CDR, US Army Research Office
ATTN: DRXRO-PH (Dr. R.J. Lontz)
PO Box 12211
Research Triangle Park, NC 27709

1 Commandant
US Army Air Defense School
ATTN: ATSA-CD-MC
Fort Bliss, TX 79916

1 Commander, DARCOM
ATTN: DRCDE
5001 Eisenhower Ave
Alexandria, VA 22333

1 Naval Surface Weapons Center
Dahlgren Laboratory
ATTN: Dr. M. Rose, Code DF-102
Dahlgren, VA 22448

1 Ballistic Missile Defense Advanced Technology Center
ATTN: Dr. L. Havard, ATC-T
P.O. Box 1500
Huntsville, AL 35807

1 Air Force Aero Propulsion Laboratory
ATTN: Mr. R. Verga, AFAPL/POD-1
Wright Patterson Air Force Base
Ohio 45433

1 Chief
Ofc of Missile Electronic Warfare
Electronic Warfare Lab, ECOM
White Sands Missile Range, NM 88002

Commander
US Army Electronics Command
Fort Monmouth, NJ 07703
1 DRSEL-GG-TD
1 DRSEL-WL-D
3 DRSEL-CT-D
1 DRSEL-TL-DT
3 DRSEL-TL-BG
1 DRSEL-TL-BG (Ofc of Record)
2 DRSEL-MS-TI
1 DRSEL-TL-D
25 Originating Office

2 MIT - Lincoln Laboratory
ATTN: Library (RM A-082)
PO Box 73
Lexington, MA 02173

1 NASA Scientific & Tech Info Facility
Baltimore/Washington Intl Airport
PO Box 8757, MD 21240

2 Advisory Group on Electron Devices
201 Varick Street, 9th Floor
New York, NY 10014

1 ITT Electron Tube Division
3100 Charlotte Avenue
Easton, PA 18042

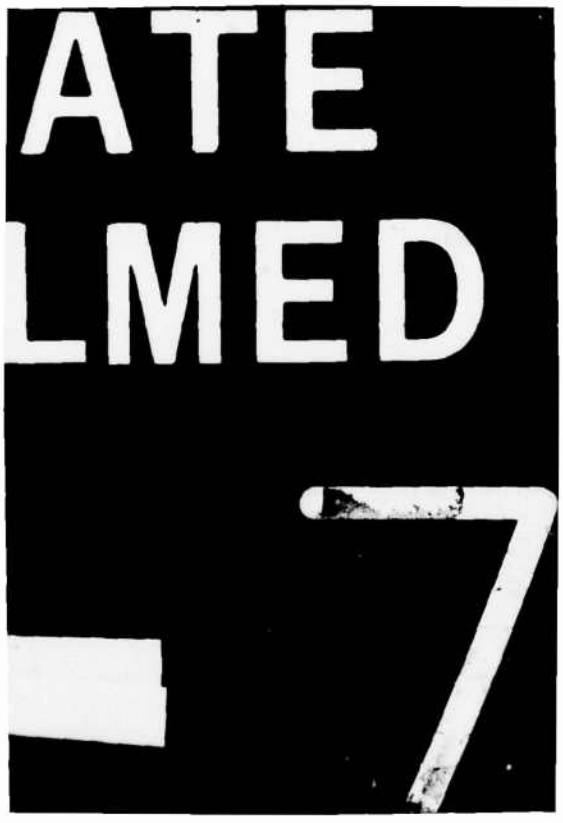
ATE
LMED
7